

Atomic carbon as a powerful tracer of molecular gas in the high-redshift Universe: perspectives for ALMA

M. Tomassetti^{1*}, C. Porciani¹, E. Romano-Diaz¹, A. D. Ludlow¹, P. P. Papadopoulos²

¹*Argelander Institut für Astronomie, Auf Dem Hügel 71, Bonn 53121, Germany*

²*University of Cardiff, School of Physics and Astronomy, Queen's Buildings, The Parade Cardiff, Wales, UK CF24 3AA United Kingdom*

Accepted 2014 ??? ?. Received 2014 ??? ?; in original form 2014 ??? ?

ABSTRACT

We use a high-resolution simulation that tracks the non-equilibrium abundance of molecular hydrogen, H_2 , within a massive high-redshift galaxy to produce mock ALMA maps of the fine-structure lines of atomic carbon $\text{C I } 1-0$ and $\text{C I } 2-1$. Inspired by recent observational and theoretical work, we assume that C I is thoroughly mixed in giant molecular clouds and demonstrate that its emission is an excellent proxy for H_2 . The entire H_2 mass of a galaxy at redshift $z < 4$ can be detected using a compact interferometric configuration with a large synthesized beam (that does not resolve the target galaxy) in less than 1 hour of integration time. Low-resolution imaging of the C I lines (in which the target galaxy is resolved into 3-4 beams) will detect nearly 50-60 per cent of the molecular hydrogen in less than 12 hours of aperture synthesis. In this case, the resulting data cube provides also the crucial information necessary for determining the dynamical state of the galaxy. We conclude that ALMA observations of the $\text{C I } 1-0$ and $2-1$ emission are well-suited for extending the interval of cosmic look-back time over which the H_2 gas mass distribution, the dynamical masses, and the Tully-Fisher relation of galaxies can be accurately probed in a seamless fashion.

Key words: galaxies: ISM - galaxies: high-redshift - ISM: molecules - methods: numerical

1 INTRODUCTION

Forbidden fine-structure lines of neutral atomic carbon can be used as tracers of the molecular mass in galaxies (Gerin & Phillips 2000; Papadopoulos et al. 2004). The ground electronic state of neutral carbon, $1s^2 2s^2 2p^2$, is split into five fine-structure levels that, in spectroscopic notation, are denoted 3P_J (with $J = 0, 1$ and 2), 1D_2 , and 1S_0 . The excited fine levels 3P_1 and 3P_2 lie only 23.6 K and 62.4 K above the ground state (3P_0) and are therefore easily populated by particle collisions in the cold interstellar medium (ISM). Two magnetic-dipole transitions are allowed between the fine-structure levels: $^3P_1 \rightarrow ^3P_0$ (which we refer to as $\text{C I } 1-0$) has a rest frequency of 492.1607 GHz, while $^3P_2 \rightarrow ^3P_1$ ($\text{C I } 2-1$) produces electromagnetic radiation at 809.3435 GHz.

Early one-dimensional models of photon-dominated regions (PDRs) confined the presence of C I to a thin transition layer separating the outer ionized zone from the CO -

rich inner volume (Kaufman et al. 1999). However, large-scale C I surveys of the Orion A and B molecular clouds (Ikeda et al. 2002) and of the Galactic center (Ojha et al. 2001) have found that the $\text{C I } 1-0$, $2-1$ line emission is fully concomitant and strongly correlates with ^{12}CO emission. In addition, several observations (e.g., Frerking et al. 1989; Schilke et al. 1995; Kramer et al. 2008) have shown that C I is ubiquitous in giant molecular clouds (GMCs). Clumpy PDR models (e.g. Spaans 1996) suggest that the surface layers of C I are evenly spread across GMCs. Moreover turbulent diffusion, cosmic-ray fluxes and non-equilibrium chemistry all help to maintain a nearly constant $[\text{C I}]/[\text{H}_2]$ abundance ratio throughout most of the mass of a typical molecular cloud (Papadopoulos et al. 2004). A recent numerical simulation of a turbulent molecular cloud confirms that C I emission should be widespread in GMCs, with most of the neutral carbon at gas densities between 10^2 and 10^4 cm^{-3} and $T_{\text{K}} 30 \text{ K}$ (Glover et al. 2014).

Sensitivity limitations but mostly the low atmospheric transmissivity in the short sub-mm regime made the detection and imaging of C I lines in the local Universe (and thus the realization that they do not conform to the standard PDR stratified picture) difficult. For objects in the distant Universe where the C I lines are redshifted in more favor-

* E-mail: mtomas@astro.uni-bonn.de

Member of the International Max Planck Research School (IMPRS) for Astronomy and Astrophysics at the Universities of Bonn and Cologne

able atmospheric windows, only a handful of galaxies have been observed between $z \sim 2 - 3$ in the 1–0 transition (Weiß et al. 2003, 2005; Alaghband-Zadeh et al. 2013, and references therein). However, this sample will likely grow with the advent of new facilities such as the Atacama Large Millimeter Array (ALMA) and the Cerro Chajnantor Atacama Telescope (CCAT). The improved sensitivity of these instruments will yield observations that significantly enhance our understanding of the molecular gas in distant galaxies and of the history of cosmic star formation.

In this letter, we use state-of-the-art simulations of galaxy formation that include an algorithm for tracking molecular gas (Tomassetti et al. 2014) to demonstrate the promise of ALMA imaging observations of the two CI fine-structure lines, with the goal of determining the molecular mass distributions of high-redshift galaxies. In a future paper we will expand our study towards dynamical mass and star formation mode studies using these lines across cosmic epoch.

2 METHODS

The simulation used in this work is presented in Tomassetti et al. (2014). Here we recap the main aspects of the run, and refer the reader to our previous paper for further details. The simulation follows the formation of a massive galaxy up to $z = 2$ using the adaptive mesh refinement code RAMSES (Teyssier 2002), achieving a physical resolution $\Delta x \simeq 180$ pc. It includes gas cooling, star formation, feedback and metal enrichment from stellar evolution. We use a novel sub-grid treatment of the formation and destruction of molecular hydrogen within unresolved GMCs to track the non-equilibrium abundance of H_2 .

Our main assumption is that atomic carbon is thoroughly mixed with molecular hydrogen and that the $[\text{C I}]/[\text{H}_2]$ abundance ratio is constant on kpc scales. This quantity is observed to range between $\sim 1 \times 10^{-5}$ and $\sim 5 \times 10^{-5}$ in non-star-forming and star-forming clouds, respectively (Frerking et al. 1989; Weiß et al. 2005; Danielson et al. 2011). In the following, we adopt the representative value of $[\text{C I}]/[\text{H}_2] \simeq 3 \times 10^{-5}$ and discuss how small changes affect our results in Section 3.

At the frequencies of the CI fine-structure lines, our simulated galaxy is optically thin and the corresponding flux density per unit frequency observed on Earth, S_{CI} , for the transition between levels u and l is

$$S_{\text{CI}} = \frac{A_{ul} h \nu_{ul} \Omega_B Q_u \bar{N}_{\text{CI}, \Delta\nu}}{4\pi (1+z)^4 \Delta\nu}. \quad (1)$$

Here A_{ul} is the Einstein coefficient, h is the Planck constant, ν_{ul} the rest-frequency of the transition, Ω_B the beam size, z the redshift of the galaxy and $\Delta\nu$ is the frequency bandwidth. The term $\bar{N}_{\text{CI}, \Delta\nu}$ denotes the beam-averaged column density of carbon atoms with line-of-sight velocities corresponding to the frequency range $\Delta\nu$ for the line transition. Lastly, $Q_u = n_u/n_{\text{CI}} < 1$ is the fractional population of level u , where n_{CI} is the total number density of atomic carbon. Given that the critical densities of the CI transitions are comparable to the densities of GMCs, it is reasonable to compute Q_u assuming local thermodynamic equilibrium (LTE). We assume a fiducial value of the gas kinetic temperature $T_k = 30$ K (e.g. Alaghband-Zadeh et al. 2013, and

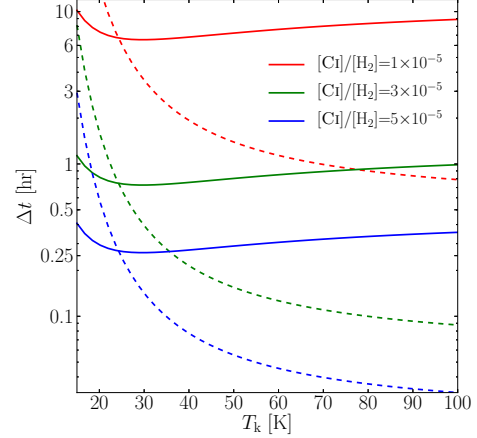


Figure 1. Integration time, Δt , required to detect the brightest pixel in the (continuum subtracted) surface-brightness map above a signal-to-noise ratio of five. This plot has been drawn for a compact ALMA configuration with a baseline length of $D = 150$ m, whose synthesized beam is larger than the simulated galaxy at any redshift.

references therein), for which $Q_1 \simeq 0.46$ and $Q_2 \simeq 0.21$, and discuss variations of T_k in Section 3.

Our current goal is to demonstrate the significant potential of ALMA CI line observations in the high- z Universe. We thus use the ALMA sensitivity calculator¹ to compute the noise level for a given integration time considering a configuration with 50 antennas for the 12-m array. Moreover, we assume that the simulated galaxies are observed at a declination $\delta = 45^\circ$ and adopt a water-vapor column density of 1.796 mm (anticipated for 62.5 per cent of observations at the ALMA site).

3 RESULTS

For a detection experiment we first consider a very compact ALMA configuration with a baseline length of $D = 150$ m. In this case, the synthesized beam is large (for observations at $z = 2$, it has a FWHM of 3.1 and 1.9 arcsec for CI 1–0 and 2–1, respectively) and the simulated galaxy is not resolved at any redshift $z > 2$. In Figure 1 we show, as a function of T_k , the integration required to detect the galaxy at $z = 2$. We integrate the data cube over the velocity range $\Delta v \simeq \pm 370$ km s^{−1}, which corresponds to four times the line-of-sight velocity dispersion of the H_2 gas in the beam, σ . We compute the integration time by requiring the brightest pixel in the (continuum subtracted) surface-brightness map to have a signal-to-noise ratio of five. For our fiducial values of the kinetic temperature and carbon abundance, 24 minutes of exposure are enough to detect the 2–1 line, while twice as much is needed for the 1–0 line. These values scale as $([\text{C I}]/[\text{H}_2])^{-2} Q_u^{-2}$ suggesting that several hours of integration are necessary for an abundance ratio of $\sim 10^{-5}$. Note that the 2–1 line is brighter than 1–0 for high gas temperatures. However, it might be difficult to detect if $T_k \ll 30$ K as the 3P_2 level may then not be significantly populated.

¹ <http://almascience.eso.org/proposing/sensitivity-calculator>

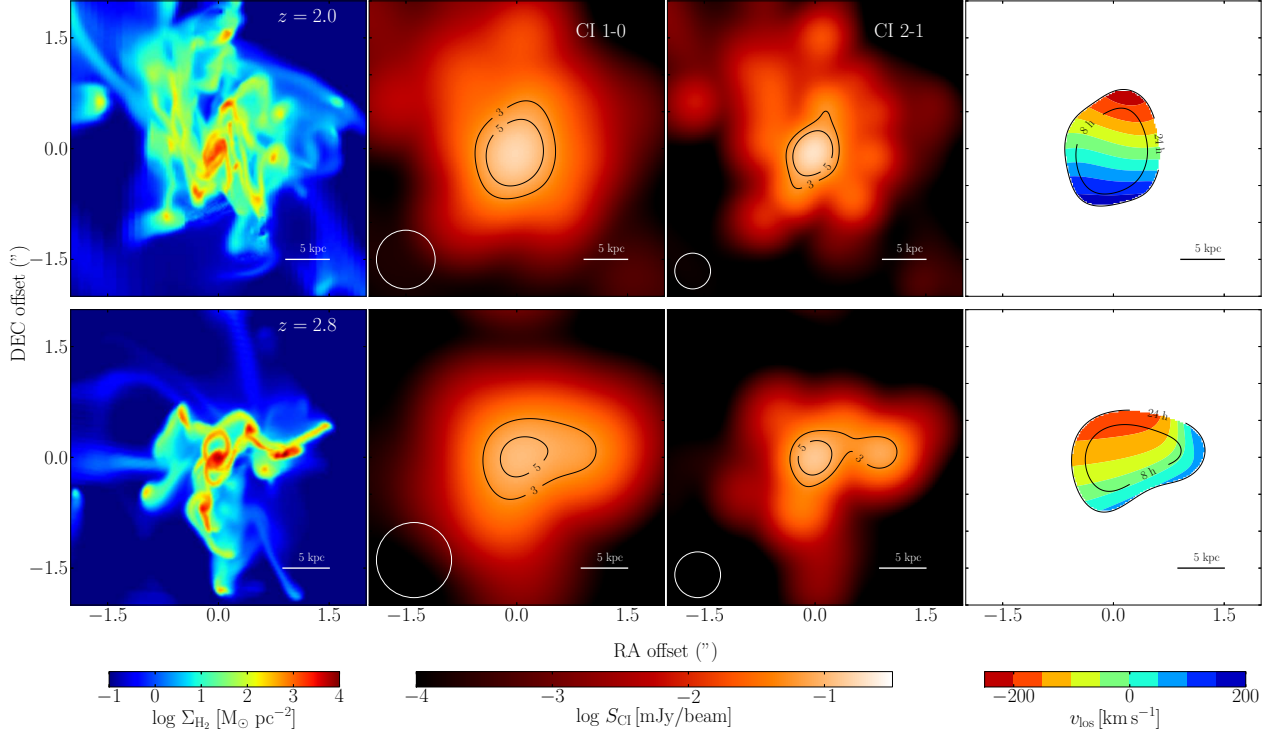


Figure 2. *Left panels:* H_2 surface density for a quiescent disk galaxy at $z = 2$ (*top row*) and a triple merger at $z = 2.8$ (*bottom row*). *Middle panels:* Flux density of the CI 1–0 (middle left) and 2–1 (middle-right) transitions for the projection shown in the left panels for a bandwidth $\Delta v = \pm 2\sigma$, a baseline $D = 700$ m and a total integration time $\Delta t = 12$ hours. Contours are drawn at S/N levels of 3 and 5; circles represent the beam size and shape. *Right panels:* Velocity maps inferred from the data cubes in velocity channels of 50 km s^{-1} . Contours show S/N=3 for different integration times.

Using equation (1), we estimate the H_2 mass contained within Ω_B using the flux in the brightest pixel, S_{CI}^{\max} :

$$M_{H_2} = \frac{4\pi m_{CI} \Delta v S_{CI}^{\max} D_L^2}{A_{ul} Q_u h c (1+z)}, \quad (2)$$

where m_{CI} is the mass of a carbon atom and D_L is the luminosity distance. Assuming perfect knowledge of both the CI temperature and the $[CI]/[H_2]$ abundance ratio, this gives at least $1.5 \times 10^{10} M_\odot$, corresponding to ~ 90 per cent of the underlying H_2 mass.

In practice, the kinetic temperature can be determined using the line-intensity ratio CI 2–1/CI 1–0 and assuming LTE (e.g. Stutzki et al. 1997). One can use also the full non-LTE $Q_u(n, T_k)$ expressions (Papadopoulos et al. 2004), provided some constraints on the average gas density (e.g. via multi-J CO and HCN lines observations) exist. On the other hand, the relative CI abundance needs to be calibrated against a statistical sample using other emission lines and measures of the dynamical mass in GMCs (e.g. from CO). Observational noise plus uncertainties in T_k and $[CI]/[H_2]$ will, of course, generate scatter around our ideal results. Finally a theoretical effort in determining the $[C/H_2]$ abundance as a function of the average SFR density is currently under way (Bisbas et al. 2014, in preparation).

The spectrum extracted from the data cube at the position of the brightest pixel can be used to extract the line-of-sight velocity dispersion, σ , and the dynamical mass of the galaxy. Between $2 < z < 3$, we find that $M_{\text{dyn}} = \alpha \sigma^2 R_B / G$ (where G is the gravitational constant and $R_B =$

$\text{FWHM}/(2\sqrt{\ln 2})$ the beam radius) with $\alpha = 3.4$ (Erb et al. 2006) yields estimates of the *total* projected mass within R_B that are accurate to ~ 15 per cent.

Next we construct low-resolution maps of the H_2 distribution within our simulated galaxy using a baseline length of $D = 700$ m. In this case, the galaxy is resolved by 3–4 telescope beams (for instance, at $z = 2$, the FWHM of the ALMA beam is of 0.7 (5.6) and of 0.4 (3.4) arcsec (kpc) for the 1–0 and 2–1 transitions, respectively) and the noise level, at $z = 2$, for an integration time Δt and a velocity bandwidth of roughly $\pm 280 \text{ km s}^{-1}$ is $\sigma_{\text{rms}} \simeq 0.06 (\Delta t/1 \text{ hr})^{-1/2} \text{ mJy/beam}$.

In Figure 2, we provide two illustrative examples of how our simulated galaxy would appear when observed with ALMA. The top panels focus on the output at $z = 2$ when the galaxy is characterized by a prominent disk (in both the stellar and gas distributions) and forms stars at a rate of $\sim 60 M_\odot \text{ yr}^{-1}$. Its stellar and H_2 masses (computed within a tenth of the virial radius of the host halo) are $M_* = 1.06 \times 10^{11} M_\odot$ and $M_{H_2} = 1.68 \times 10^{10} M_\odot$, respectively. The bottom panels, instead, consider a merger at $z = 2.8$, during which the total stellar ($M_* = 8.9 \times 10^{10} M_\odot$) and molecular hydrogen ($M_{H_2} = 2.6 \times 10^{10} M_\odot$) masses are distributed amongst three roughly equal-mass objects. In this case, the star-formation rate of the system is of $95 M_\odot \text{ yr}^{-1}$.

In the left-hand panels, we plot the H_2 surface density at the spatial resolution of the simulation (for a line of sight that forms an angle of 45 degrees with respect to the $z = 2$ disk). Central panels show the corresponding CI flux densi-

ties for the 1–0 and 2–1 transitions. In order to detect the brightest pixel in the maps with a signal-to-noise (S/N) ratio of 3 (5) one would require an integration time of ~ 1 (3) hours for both transitions in the quiescent disk case. For the merging system, the corresponding integration times are ~ 3 (8) hours and ~ 2 (5) hours for the 1–0 and 2–1 transitions, respectively. Signal-to-noise contours (solid lines) drawn for an integration time of 12 hours reveal that the detectable signal originates from regions where the beam-averaged H_2 column density is, on average, $\sim 150 \text{ M}_\odot \text{ pc}^{-2}$.

In the right panel we plot the velocity map constructed by averaging the data cube in the direction of the line of sight and using velocity channels of 50 km s^{-1} . Contours of $\text{S/N}=3$ are drawn for different integration times and show that $\Delta t = 8 \text{ hr}$ is sufficient to retrieve detailed dynamical information.

It is useful to estimate how accurately we can reconstruct the H_2 mass of the galaxy from resolved imaging of the C1 1–0 and 2–1 line intensities. To do so, we compute the total H_2 mass that occupies the same volume as the observable carbon atoms. This is achieved by convolving the H_2 surface-density maps with the ALMA beam and integrating over the solid angle subtended by regions in which S_{C1} is above a given flux limit, S . In the left-hand panel of Figure 3, we show our results for the galaxy at $z = 2$ (a similar trend is found for the merging system). The recovered H_2 mass increases with decreasing the flux limit. For an integration time of 12 hours, the H_2 fraction recovered from the area over which S_{C1} is above $3\sigma_{\text{rms}}$ (hereafter $f_{\text{H}_2}^{\text{rec}} = M_{\text{H}_2}^{3\sigma}/M_{\text{H}_2}$) is ~ 57 and ~ 43 per cent for the 1–0 and 2–1 transitions, respectively. Integrating longer or reducing the baseline length boosts signal from the less dense regions. For example, $f_{\text{H}_2}^{\text{rec}}$ increases to ~ 85 (for C1 1–0) and ~ 76 (for C1 2–1) per cent for $D = 400 \text{ m}$. Finally, we note that the low surface density of H_2 outermost regions of the galaxy require prohibitively long integration times to be detected. Fortunately, these regions only contain a few per cent of the total molecular mass in our simulation.

Finally, we measure the redshift-dependence of the H_2 mass fraction that can be recovered (above $3\sigma_{\text{rms}}$) from C1 observations. This is achieved by following back in time the most massive progenitor of the $z = 2$ dark matter halo and imaging a region surrounding its central galaxy. Results are plotted in Figure 4 and show that, for the compact baseline of 150 m, the entire H_2 mass within the galaxy can be detected up to $z \sim 4$ with an integration time $\Delta t < 12$ hours. The mass ratio $f_{\text{H}_2}^{\text{rec}}$ is often greater than unity because the large beam collects additional signal from regions outside the galaxy (which, in our simulations, has a radius of $\sim 12.6 \text{ kpc}$ at $z = 2$) which also contain molecular hydrogen. Instead, for a baseline length of 700 m, roughly half of the H_2 mass can be recovered in the same redshift range. At higher redshifts, detection of H_2 with the C1 transition becomes difficult. This is due to a combination of two effects. First, the H_2 mass is lower at high redshift: it rises from 10^9 M_\odot to 10^{10} M_\odot between $z = 6$ and 3, and afterward remains roughly constant to $z = 2$. Second, the ALMA sensitivity changes in the different bands. For instance, it is impossible to observe the 2–1 transition at $z \sim 3.4$ because of the presence of a strong atmospheric water-vapor line at 183 GHz. Similarly, the 1–0 line cannot be observed around

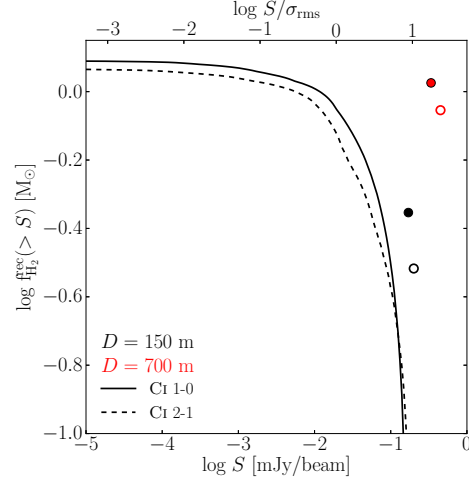


Figure 3. Lines show the molecular hydrogen mass, normalized to the total H_2 mass in the galaxy, obtained by integrating over a solid angle subtended by regions in which S_{C1} is above a given flux limit, S , for the 1–0 (solid line) and 2–1 (dashed line) transitions. Symbols indicate the flux in the brightest pixel and the corresponding H_2 mass contained within Ω_B as inferred from equation (2) for the 1–0 (filled circles) and 2–1 (empty circles) transitions. Results are plotted for the case with $D = 700 \text{ m}$ (black lines and symbols) and $D = 150 \text{ m}$ (red symbols). The upper x-axis shows the corresponding signal-to-noise ratio for the 1–0 transition (and integration time $\Delta t = 12$ hours). For this plot we have assumed $[\text{C1}]/[\text{H}_2] = 3 \times 10^{-5}$ and $T_k = 30 \text{ K}$.

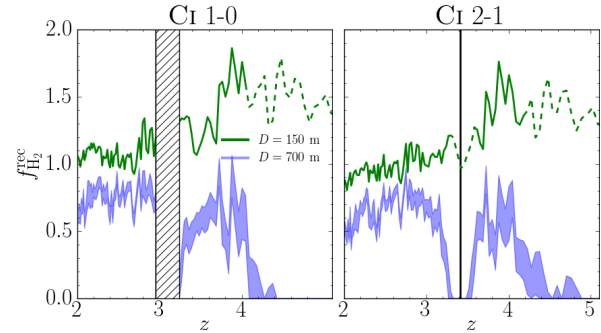


Figure 4. Fraction of H_2 mass recovered (above $3\sigma_{\text{rms}}$) from the main galaxy in our simulation as a function of redshift for $D = 700 \text{ m}$ and an integration time ranging from 12 to 24 hours (purple shades). The green line shows the recovered H_2 fraction from the brightest pixel in the image for the case with $D = 150 \text{ m}$. The dashed segments indicate redshifts at which the integration time required to detect the peak flux exceeds 12 hours. The hatched region in the left panel indicates the gap between Bands 3 and 4 in the ALMA setup, while the vertical line in the right panel marks the strong atmospheric water line at 183 GHz.

$z \sim 3$ due to a gap between Bands 3 and 4 in the ALMA setup.

4 CONCLUSIONS

We have used a high-resolution simulation that follows the formation and evolution of a massive galaxy at $z > 2$ as a template for future ALMA observations of the fine-structure

C I lines. Our simulation includes a sophisticated algorithm to track the non-equilibrium abundance of molecular hydrogen, accounting for its creation on dust grains and destruction by the Lyman-Werner photons emitted by young stars.

Assuming a characteristic value of 3×10^{-5} for the $[C I]/[H_2]$ abundance ratio and a C I excitation temperature of 30 K, we find that ALMA should be able to detect our galaxy in less than one hour integration time in its most compact configuration. Longer observations will be required to draw low-resolution maps (with a FWHM of a few arcsec) of the column density of neutral carbon while integration times become prohibitively long for small beam sizes.

If C I is well-mixed with H_2 , as recent models and local observations suggest, an integration time of 1 hr (for a compact baseline length of 150 m) will be sufficient to detect the C I emission coming from the regions where the vast majority of H_2 mass lies at redshifts $z < 3$. The resulting recovered H_2 fractions do not depend on the dynamic state of the galaxy: observing violent mergers and quiescent disks give comparable results. Based on this, we conclude that the fine-structure C I lines can be used as a reliable tracer of molecular hydrogen at $z < 3$.

For more distant galaxies, the C I signal can be detected only from the densest regions that contain a lower fractions of the molecular mass. For instance, our results indicate that only 40-50 per cent of the total H_2 mass in the galaxy can be recovered at $z = 4$. At higher redshifts the fraction of the molecular mass that is reconstructed from the C I lines drops dramatically.

Using the C I fine-structure lines as tracers of the H_2 distribution provides several advantages over more traditional studies employing rotational transitions of carbon monoxide. First, the C I lines have a strong positive K-correction with respect to the low- J CO transitions but similar excitation characteristics that still allow them to probe the bulk of the H_2 mass (Papadopoulos et al. 2004). On the other hand, the two high- J CO lines with similar frequencies to the C I lines (CO $J=4-3$, 7-6), while often bright in star-forming galaxies, mark *only* the dense and warm H_2 gas in star-forming regions. Therefore, they do not sample the entire H_2 gas distribution, and typically enclose much more compact galactic regions.

Finally, some words regarding the much brighter C II line which has been recently detected with ALMA in a gaseous starbursting disk out to $z \sim 5$ (De Breuck et al. 2014). Its emission, while much brighter than C I, it is not tied to the H_2 gas alone but also to the H I and H II distributions, which are currently unknown in high-redshift galaxies (and will remain so until the advent of SKA). Moreover its very high frequency of ~ 1900.54 GHz makes interferometric imaging observations at $z \lesssim 2$ rather challenging, even with ALMA. We note that high-fidelity, phase-stable imaging of gas-rich disks at high redshift is necessary for tasks such as determining their dynamical mass.

Thus the two lower-frequency C I lines carry several advantages as tracers of H_2 gas and the enclosed dynamical-mass across cosmic time. Furthermore, when combined with transitions that trace only dense star-forming gas (e.g. CO 4-3, HCN 1-0), they can also provide a powerful probe of the star-formation mode (isolated disk versus merger-driven) in the Universe (Papadopoulos & Geach 2012), a potential which we will be exploring in a future paper.

We conclude that using the two C I lines (rather than low- J CO lines) opens up a much larger fraction of cosmic look-back time over which the H_2 gas mass distribution, the dynamical masses, and the Tully-Fisher relation of galaxies can be seamlessly probed.

ACKNOWLEDGEMENTS

We thank Nadya Ben Bekhti for fruitful discussions. This work was supported by the DFG through the project SFB 956 *Conditions and Impact of Star Formation*. MT was supported through a stipend from the IMPRS in Bonn and PPP was supported through an Ernest Rutherford Fellowship from STFC. We acknowledge that the results of this research have been achieved using the PRACE-2IP project (FP7 RI-283493) resources HeCTOR based in the UK at the UK National Supercomputing Service and the Abel Computing Cluster based in Norway at the University of Oslo.

REFERENCES

- Alaghband-Zadeh S., Chapman S. C., Swinbank A. M., Smail I., et al. 2013, MNRAS, 435, 1493
- Danielson A. L. R., Swinbank A. M., Smail I., Cox P., et al. 2011, MNRAS, 410, 1687
- De Breuck C., Williams R. J., Swinbank M., Caselli P., et al. 2014, ArXiv:1404.2295
- Erb D. K., Steidel C. C., Shapley A. E., Pettini M., et al. 2006, ApJ, 646, 107
- Frerking M. A., Keene J., Blake G. A., Phillips T. G., 1989, ApJ, 344, 311
- Gerin M., Phillips T. G., 2000, ApJ, 537, 644
- Glover S. C. O., Clark P. C., Micic M., Molina F., 2014, ArXiv e-prints
- Ikedo M., Oka T., Tatematsu K., Sekimoto Y., et al. 2002, ApJS, 139, 467
- Kaufman M. J., Wolfire M. G., Hollenbach D. J., Luhman M. L., 1999, ApJ, 527, 795
- Kramer C., Cubick M., Röllig M., Sun K., et al. 2008, A&A, 477, 547
- Ojha R., Stark A. A., Hsieh H. H., Lane A. P., et al. 2001, ApJ, 548, 253
- Papadopoulos P. P., Geach J. E., 2012, ApJ, 757, 157
- Papadopoulos P. P., Thi W.-F., Viti S., 2004, MNRAS, 351, 147
- Schilke P., Keene J., Le Bourlot J., Pineau des Forets G., Roueff E., 1995, A&A, 294, L17
- Spaans M., 1996, A&A, 307, 271
- Stutzki J., Graf U. U., Haas S., Honingh C. E., et al. 1997, ApJL, 477, L33
- Teyssier R., 2002, A&A, 385, 337
- Tomassetti M., Porciani C., Romano-Diaz E., Ludlow A. D., 2014, ArXiv:1403.7132
- Weiß A., Downes D., Henkel C., Walter F., 2005, A&A, 429, L25
- Weiß A., Henkel C., Downes D., Walter F., 2003, A&A, 409, L41